Supplementary information for

Phytic acid controlled in situ synthesis of amorphous cobalt phosphate/carbon composite as anode materials with a high mass loading for symmetrical supercapacitor: Amorphization of the electrode to boost the energy density

Taewoo Kim,[a] Arjun Prasad Tiwari,[a,b]* Kisan Chhetri,[a] Gunendra Prasad Ojha,[a] Hyoju Kim,[a] Su-Hyeong Chae,[a] Bipeen Dahal,[a] Byoung Min Lee,[c] Tanka Mukhiya,[a] Hak Yong Kim[a,d] *

[a]Department of BIN Convergence Technology, Jeonbuk National University, Jeonju 561-756, Republic of Korea

[b]Carbon Nano Convergence Technology Center for Next Generation Engineers (CNN), Jeonbuk National University, Jeonju, Republic of Korea

[c]Department of Carbon Materials and Fiber Engineering, Jeonbuk National University

[d]Department of Organic Materials and Fiber Engineering, Jeonbuk National University, Jeonju 561-756, Republic of Korea

*Corresponding author: E-mail address: tiwariarjuna@jbnu.ac.kr/tiwariarjuna@gmail.com (A.P. Tiwari); khy@jbnu.ac.kr (H.Y. Kim)

Synthesis of the GC@CoPi-CC

The glucose-derived carbon sample with a CoPi-loaded CC was prepared by a conventional phosphorization method for comparative study and is referred to as GC@CoPi-CC. Glucose replaced PA as the carbon precursor, and NaH_2PO_2 was used as the phosphorus source. Briefly, metallic Co was attached to the CC by simple carbonization of the CC with cobalt acetate (0.18 mM) at 800 °C under a N_2 atmosphere.[1] Later, the sample was placed into a glucose solution (0.36 mM) followed by heating (250 °C at 2 °C/minute for 2 h under 40 cm^3/minute Ar flow) in a tube furnace along with NaH_2PO_2 on the upstream side. The resulting sample is referred to as GC@CoPi-CC. The loading amount of the active material was estimated to be 2 mg cm^{-2}.

Physicochemical characterization

The morphologies of the CCs after active material loading were evaluated by field emission scanning electron microscopy (FESEM) and high resolution transmission electron microscopy (HRTEM, JEM–2100F, Japan). To study the crystallinity of the materials, X-ray diffraction (XRD, Rigaku Co., Japan) was used at 100 kV. X-ray photoelectron spectrometry (Thermo Scientific ESCALAB 250Xi, USA) with Al Kα radiation (λ = 8.34 Å) as the excitation source was employed to study the surface elements of the samples. N_2 adsorption and desorption isotherm analyses were conducted on a Quantachrome Autosorb–iQ sorption analyzer at liquid N_2 temperature, and the specific surface area was calculated by using the Brunauer–Emmett–Teller (BET) method. Raman spectra were collected on a confocal laser micro–Raman spectrometer (Renishaw, UK) with an excitation of 532 nm. The wettability was determined by measuring the contact angles on a contact angle analyzer (GBX, Digidrop, France) by dropping 2 μL of deionized water onto the surfaces of the CCs.

Supplimetary results

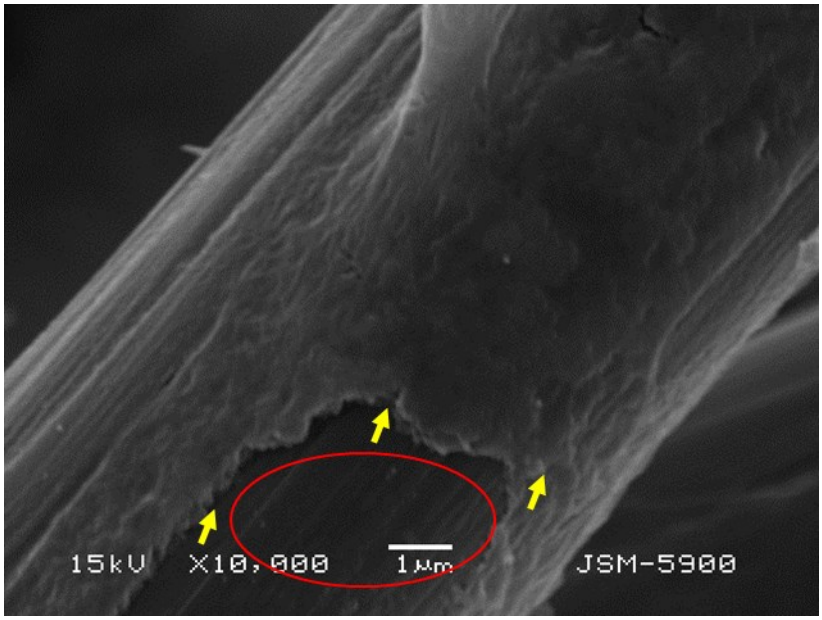

Figure S1. *SEM image of an individual fiber of a-PC@CoPi-CC. Arrows showing the CoPi/C layer while the red circle shows the part of CC after removing the coated layer.*

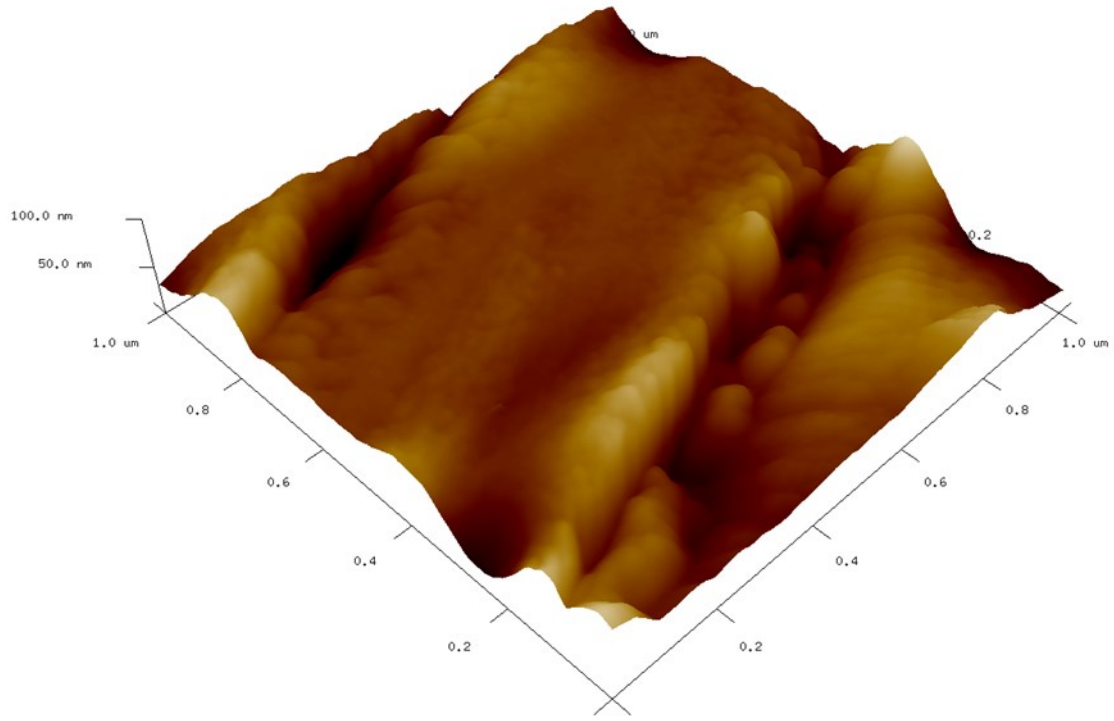

Figure S2. *AFM image of the a-PC@CoPi-CC8.*

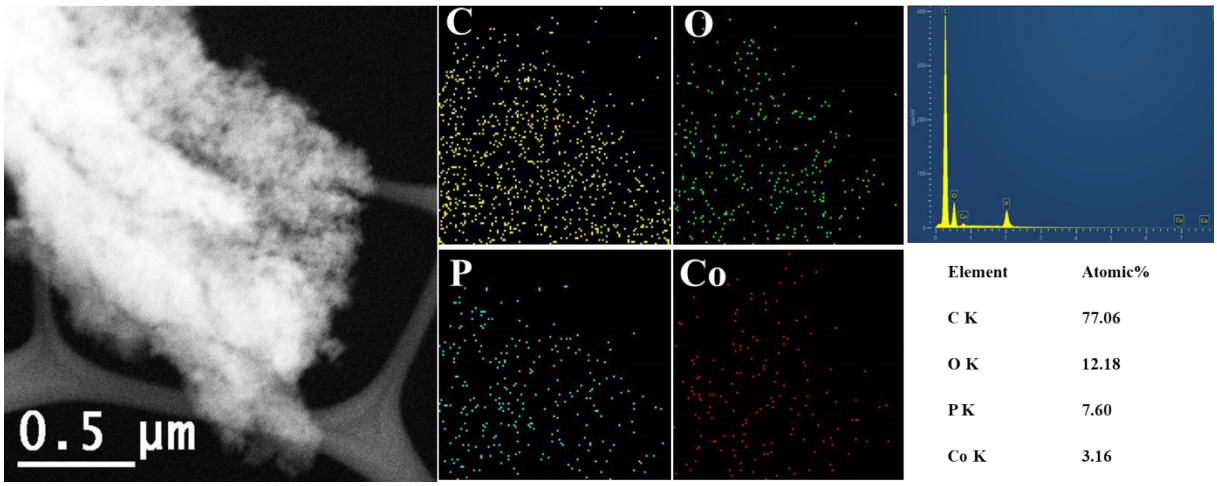

Figure S3. *STEM image and its corresponding elemental mapping images and EDX spectra of a-PC@CoPi-CC8.*

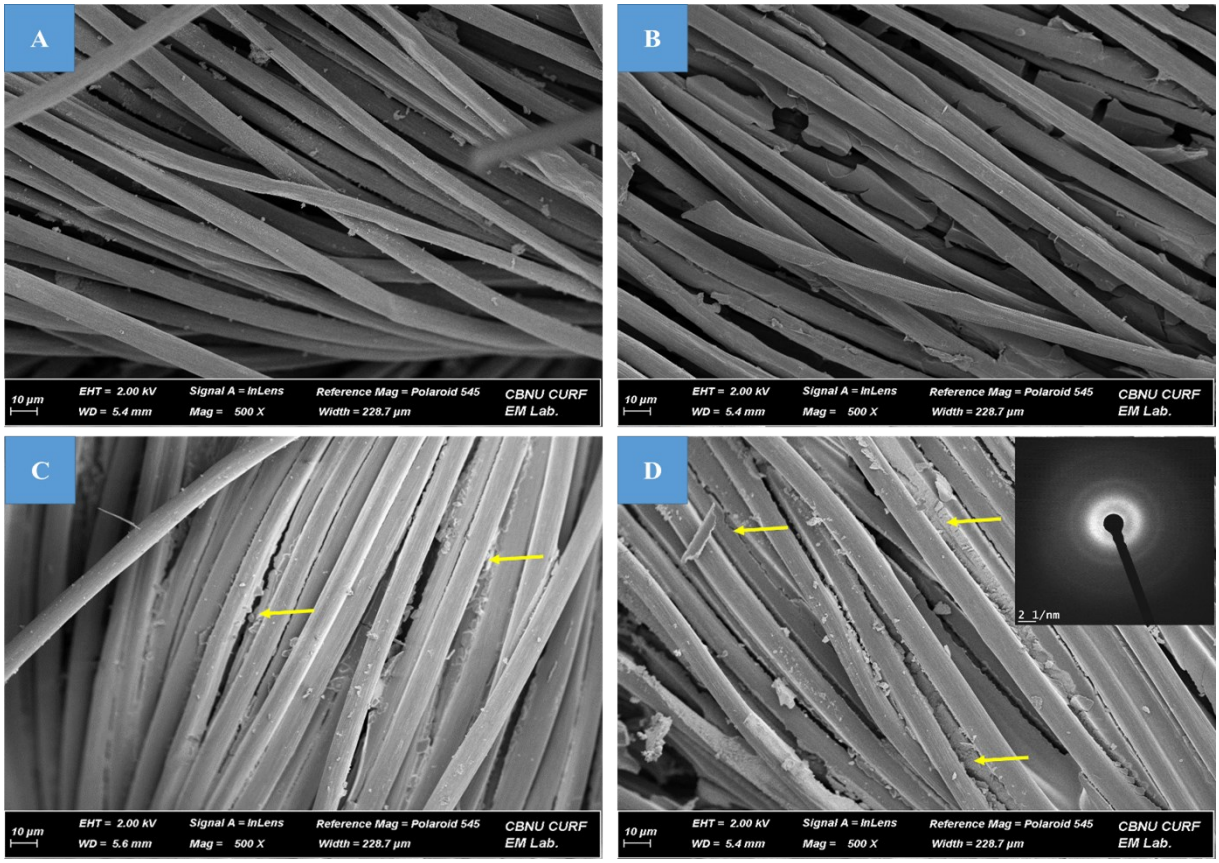

Figure S4. *FE-SEM images of the a–PC@CoPi-CC2 (A), a–PC@CoPi-CC5 (B), a–PC@CoPi-CC8 (C), and a–PC@CoPi-CC12 (D). The inset of 'D' shows the TEM-SAED of a–PC@CoPi-CC12 sample.*

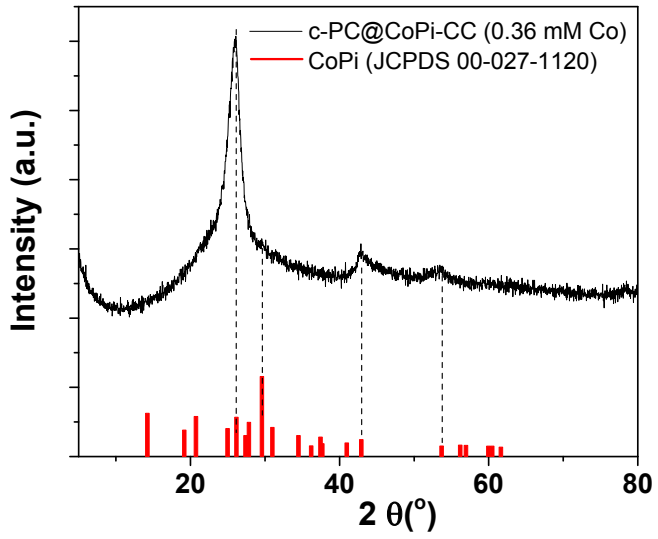

Figure S5. *XRD spectrum of a sample prepared from the cobalt acetate of 0.36 mM.*

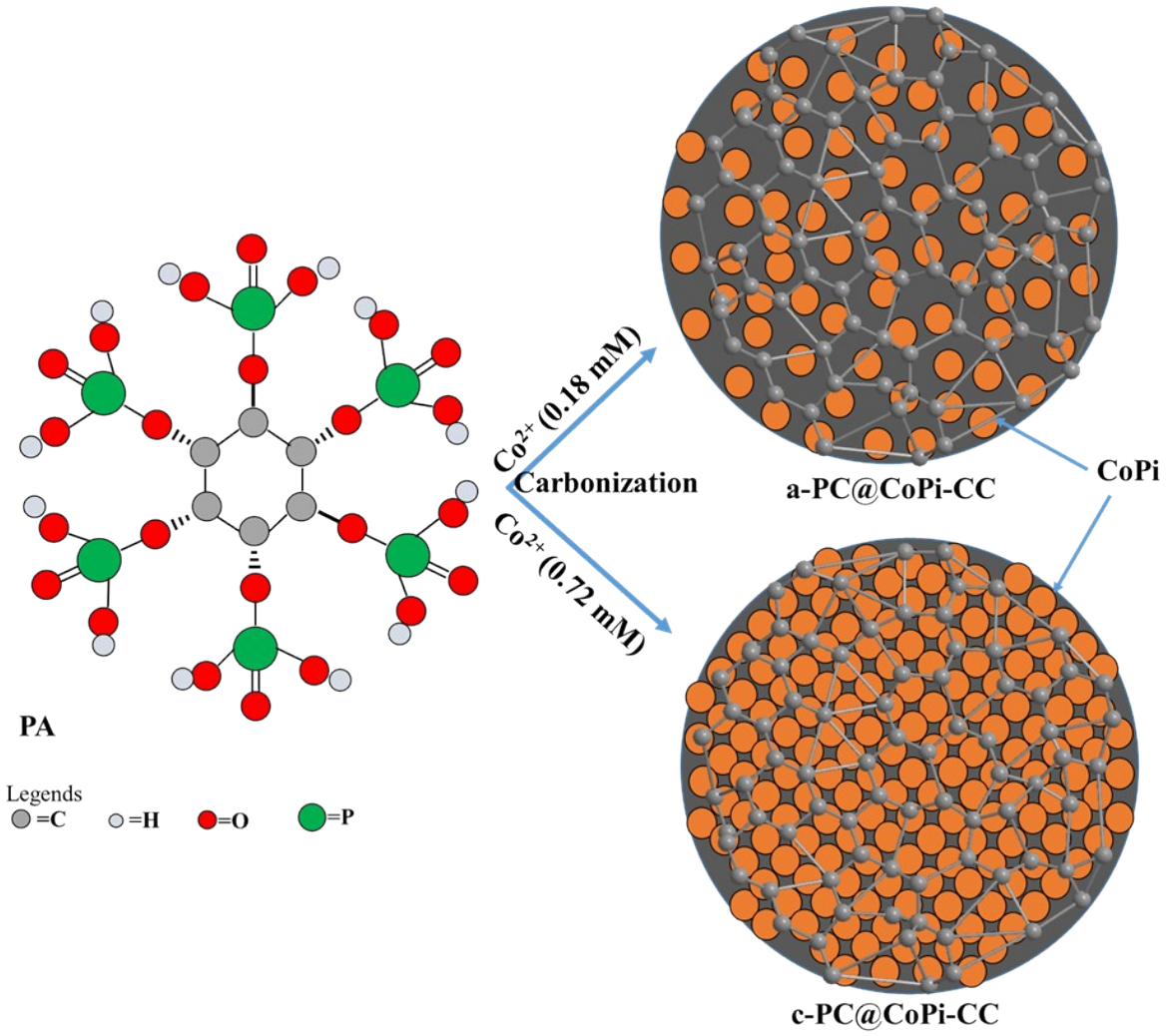

Figure S6. *Schematic illustration of conditions showing the synthesis of amorphous (a-PC@CoPi-CC) and crystalline (c-PC@CoPi-CC) samples.*

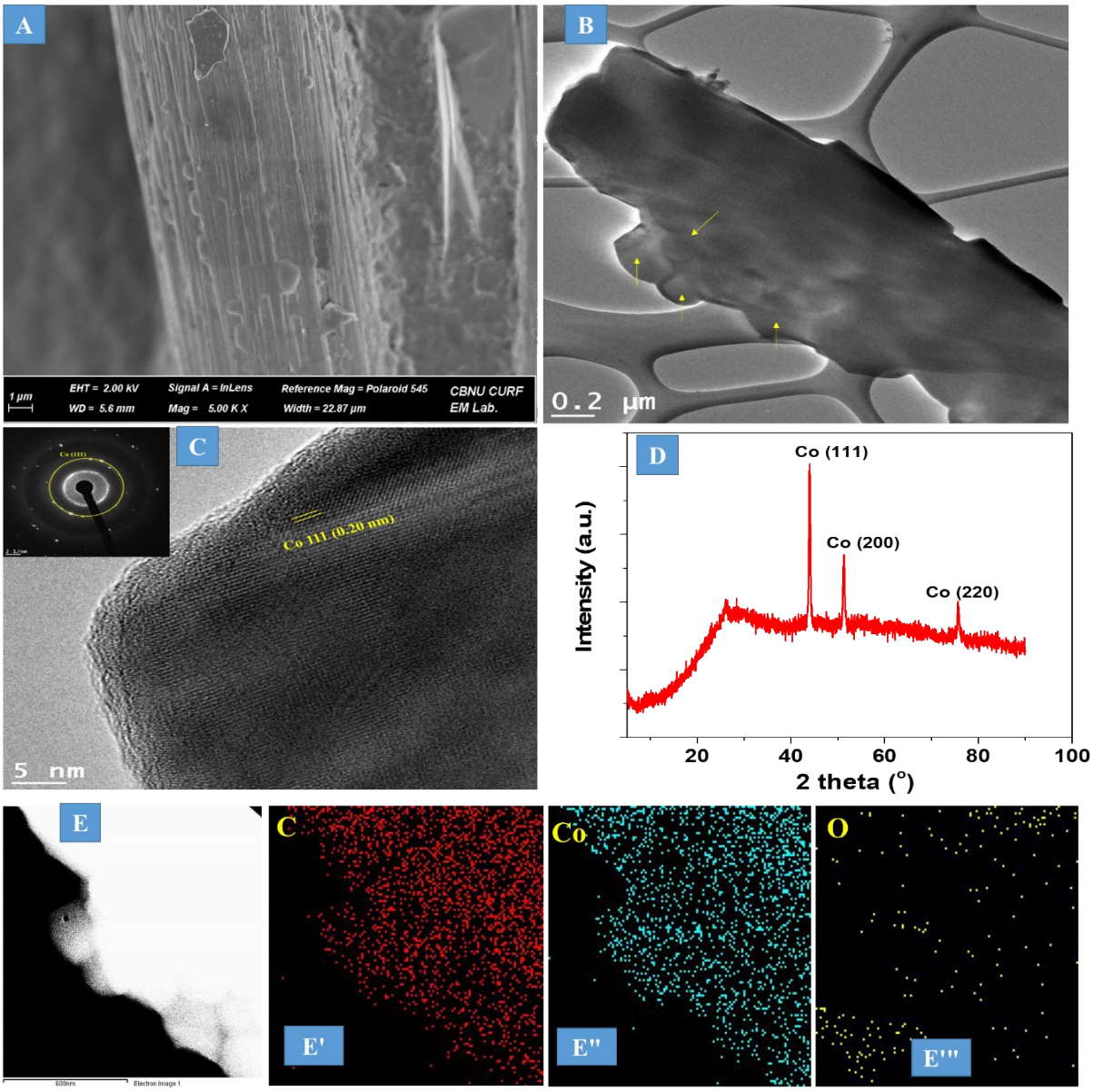

Figure S7*. FE-SEM image (A), TEM image (B-C), arrows of B show the particles attached to the carbon fiber. SAED pattern of corresponding TEM image (inset of C), XRD spectrum (D), and STEM image and its corresponding elemental mapping images (E) of GC@Co-CC.*

The FESEM image shows that the particles were deposited on the carbon fiber (**Figure S7A**).The HRTEM image further confirms that particles of 100-300 nm in diameter adhered to the substrate (**Figure S7B**). The crystal planes (111) with a d-spacing of 0.20 nm can be directly observed (**Figure S7C**). The corresponding SAED pattern also matched well with the HRTEM d-spacing data. The XRD pattern for the GC@Co-CC exhibits peaks at 44.0° ((111) plane),

51.3° ((200) plane) and 76.1° ((220) plane) that correspond to crystalline cobalt (**Figure S7D**). The EDX mapping images of the HRTEM images are shown in Figure S7E.

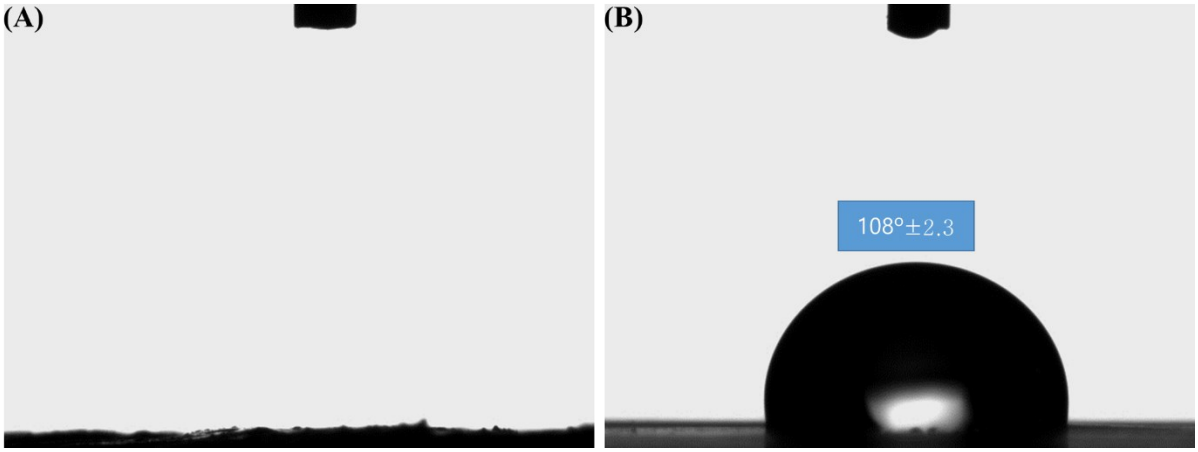

Figure S8. *The contact angle of CC with PA/ethanol (1:1) (A) Water/ethanol (1:1) (B). 'A' condition was applied to make phytic acid-derived structures (a-PC@CoPi-CC) while 'B' was to the synthesis of GC@Co-CC and GC@CoPi-CC.*

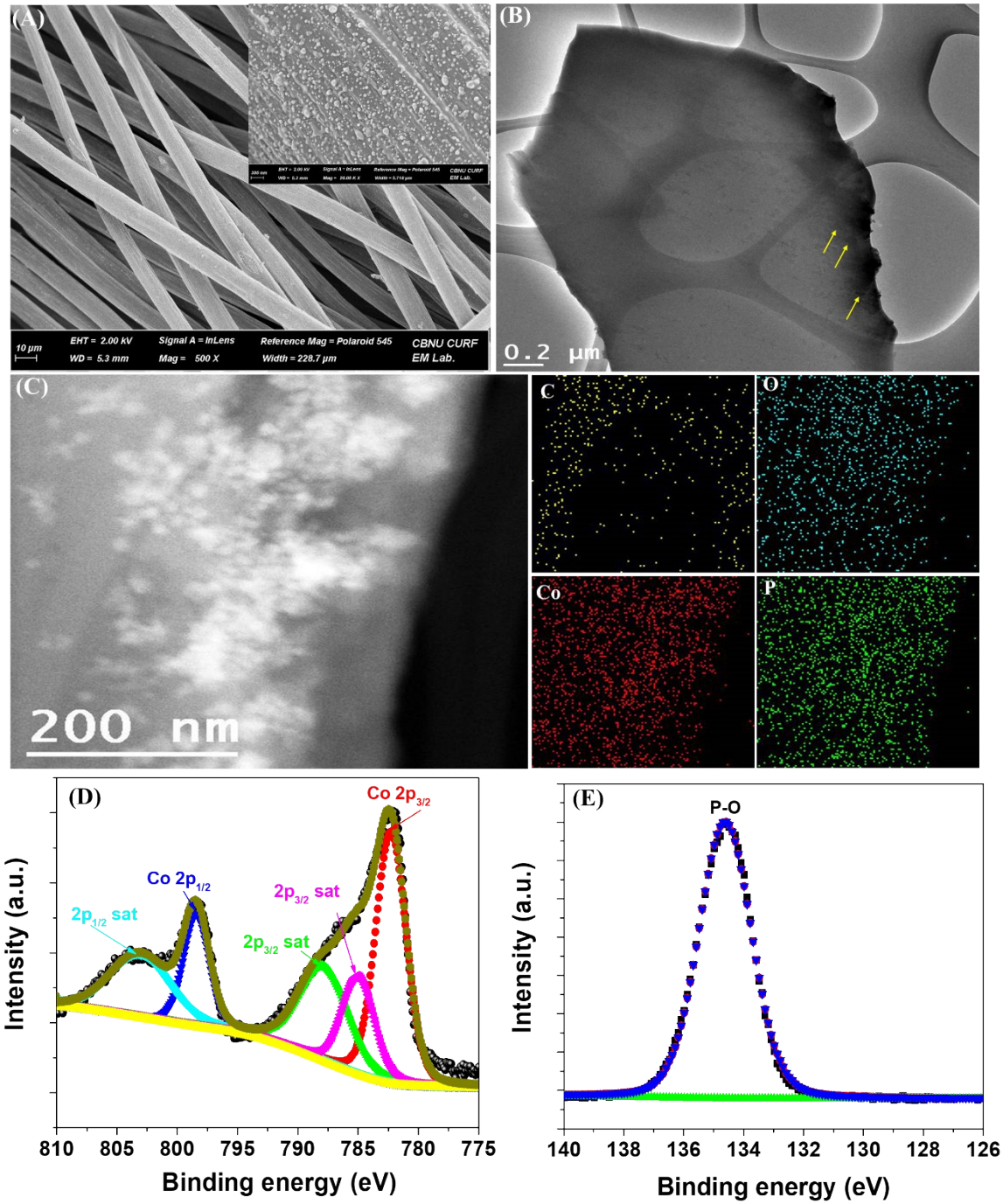

Figure S9. *FESEM image (A), HR-TEM-image, arrows show the particles (B), STEM image, and corresponding elemental mapping images (C). STEM image analysis revealed the presence of all expected major elements, namely, C, O, Co, and P. XPS spectrum of GC@CoPi-CC (D,E). High-resolution XPS spectra of Co 2p show peaks centered at 782.3 and 798.4 eV are attributed to Co $2p_{3/2}$ aSnd Co $2p_{1/2}$, respectively of oxidized cobalt.*[2] *The binding energy located at 134.6 eV can be ascribed to the +5 state for all P atoms in the product P 2p.*[3]

Therefore, the XPS analysis confirms the formation of cobalt phosphate. According to XPS data, the atomic wt% of C, O, P, and Co are found 57.07, 29.23, 10.33, and 3.37%, respectively.

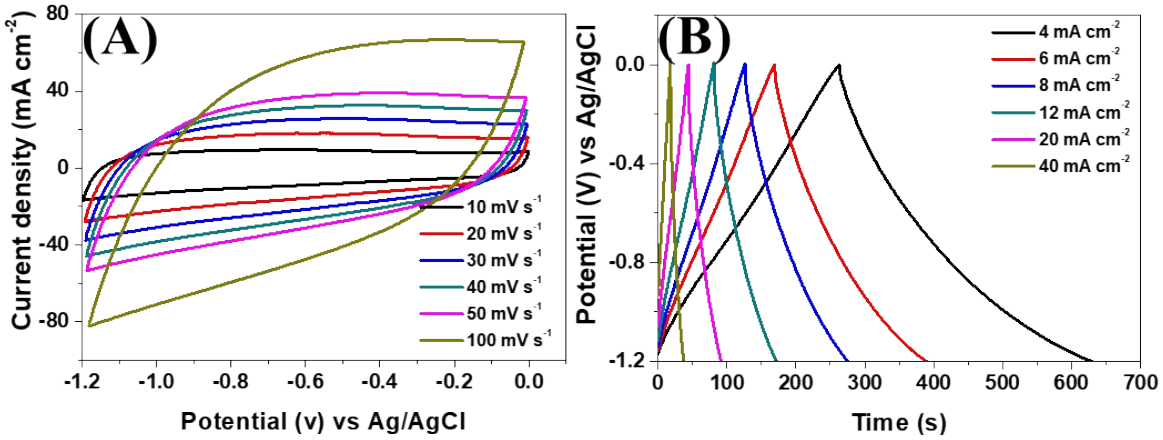

Figure S10. *CV (A), and GCD (B) curves of the a-PC@CoPi-CC2.*

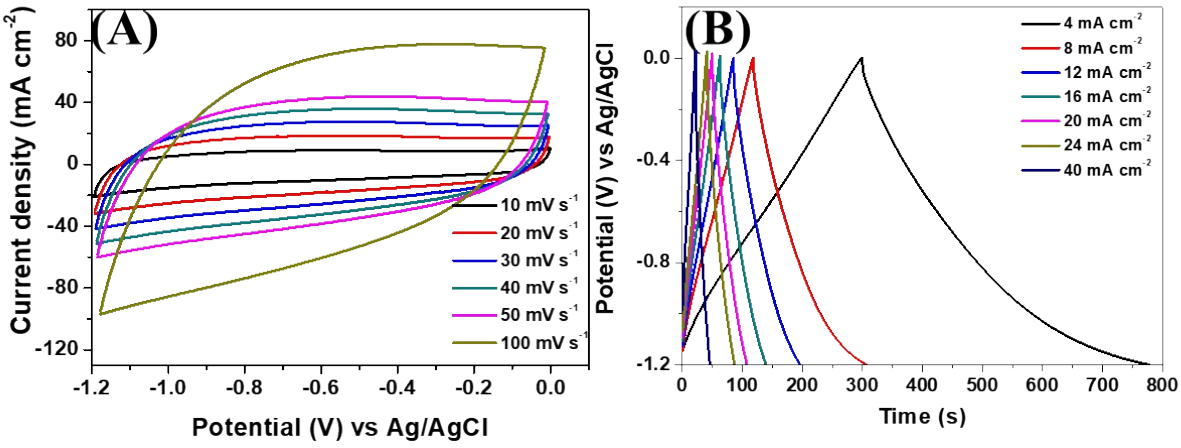

Figure S11. *CV (A), and GCD (B) curves of the a-PC@CoPi-CC5.*

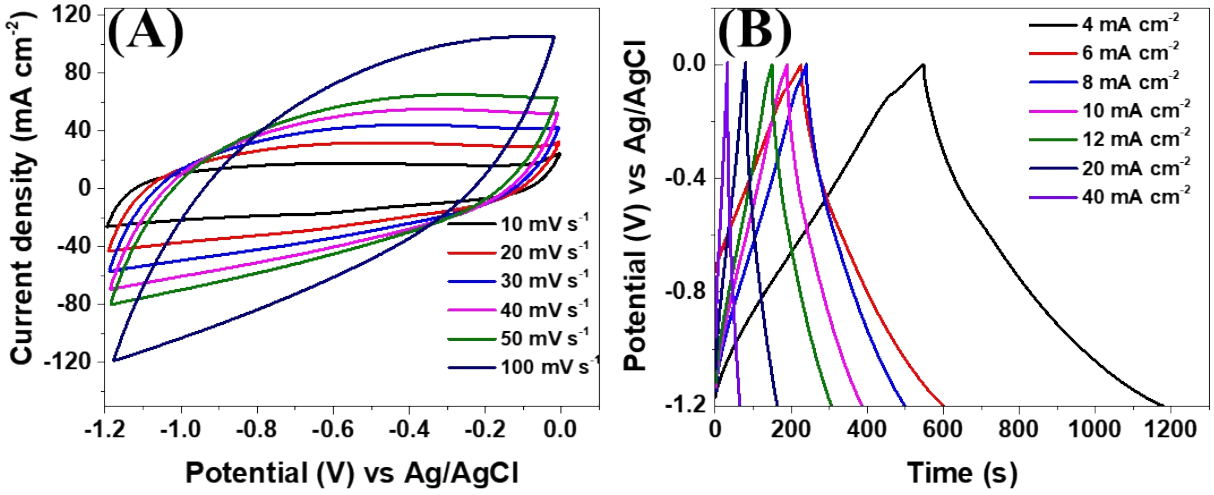

97

98 ***Figure S12****. CV (A), and GCD (B) curves of the a-PC@CoPi-CC12.*

99

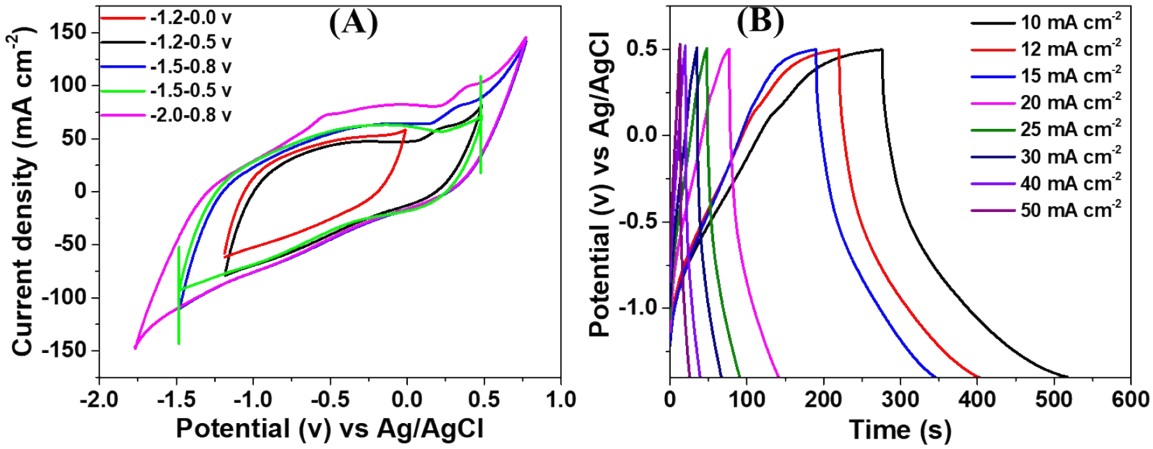

100

101 ***Figure S13.*** *CV curves of a-PC@CoPi-CC8 at the different potential window at 50*

102 *mV* s^{-1} *(A) and GCD curves of the same sample at different current densities at*

103 *potential ranges from -1.4 to 0.5 (B).*

104

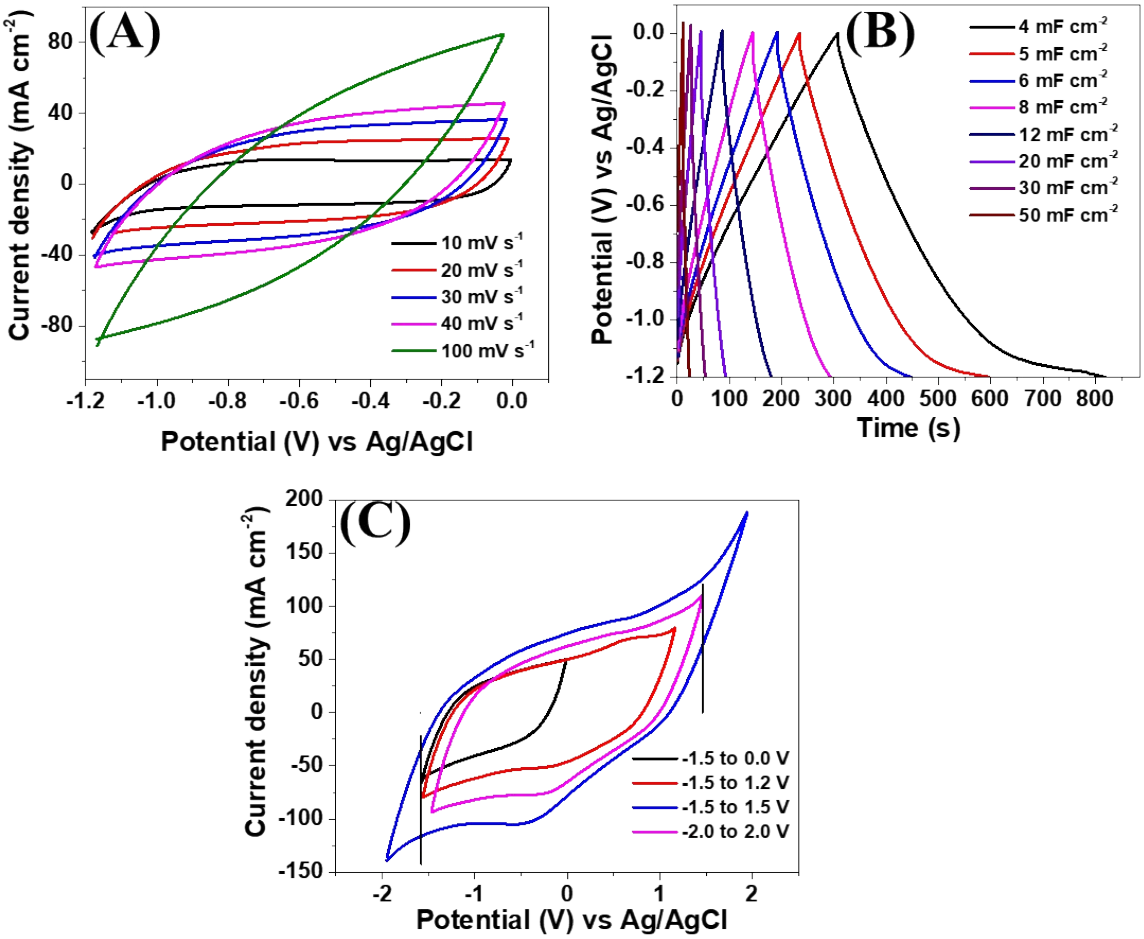

105

106 ***Figure S14.*** *CV (A), GCD (B) curves of a-PC@CoPi-CC8 in 1 M Na_2SO_4 and CV curves*

107 *showing the maximum possible working potential window ranges of a-PC@CoPi-CC8 in a 1*

108 *M Na_2SO_4 (C).*

109

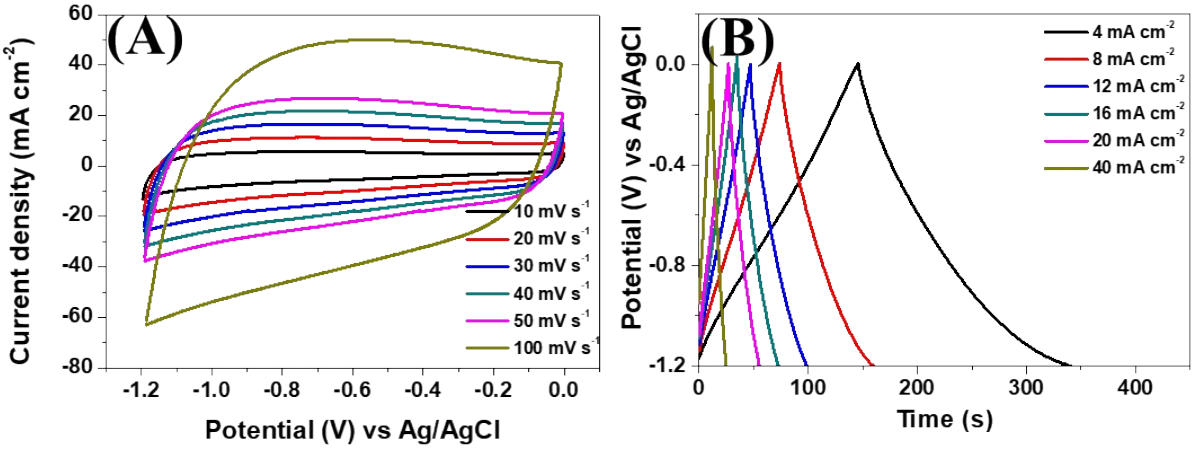

Figure S15. *CV (A), and GCD (B) curves of PC@CC. The loading amount is estimated to be 5 mg cm^{-2}.*

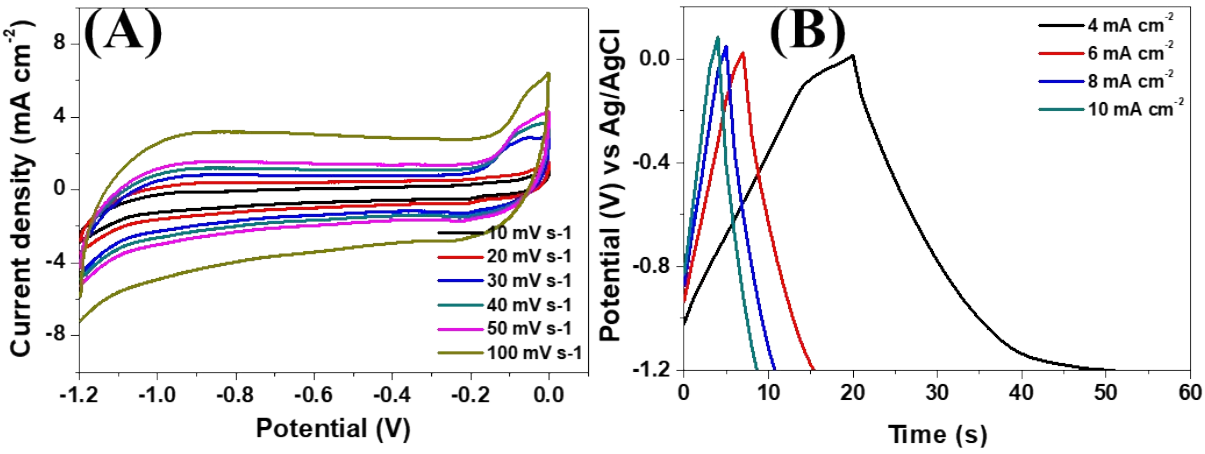

Figure S16. *CV (A) and GCD (B) curves of GC@Co-CC. The loading amount is estimated to be 2 mg cm^{-2}.*

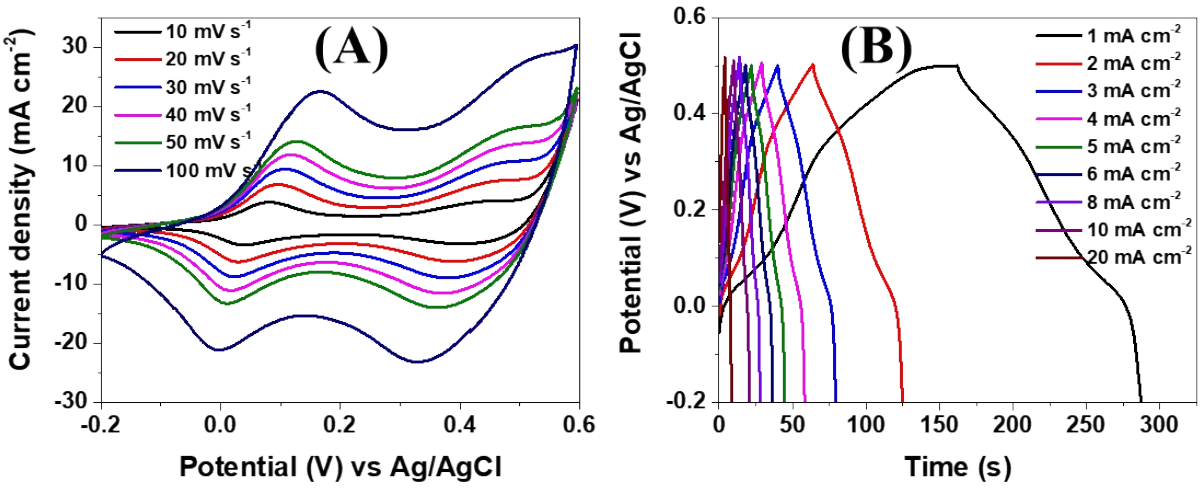

119

120 ***Figure S17.*** *CV (A) and GCD (B) curves of GC@CoPi-CC. The loading amount is estimated*

121 *to be 2 mg cm*$^{-2}$.

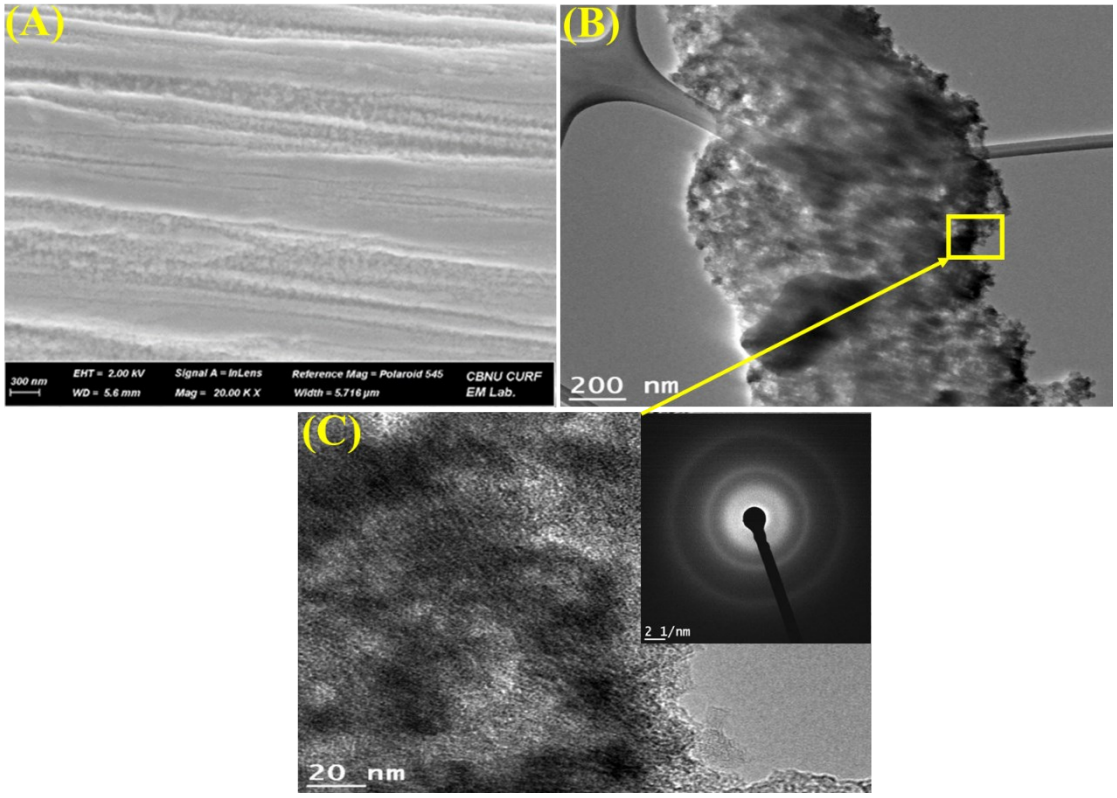

122

123 ***Figure S18.*** *SEM image (A), TEM images of a-PC@CoPi-CC8 after the cyclic stability test*

124 *(B, C). Inset (C) shows the SAED pattern of the corresponding TEM image.*

125

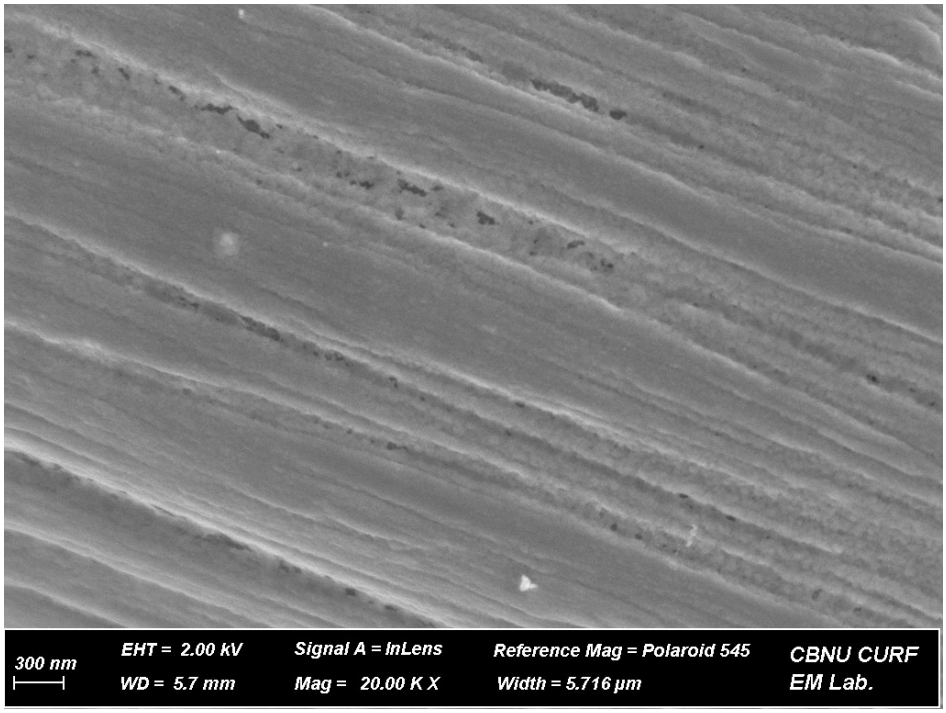

126

127 ***Figure S19.*** *SEM image of the a-PC@CoPi-CC8 after 30 min of sonication.*

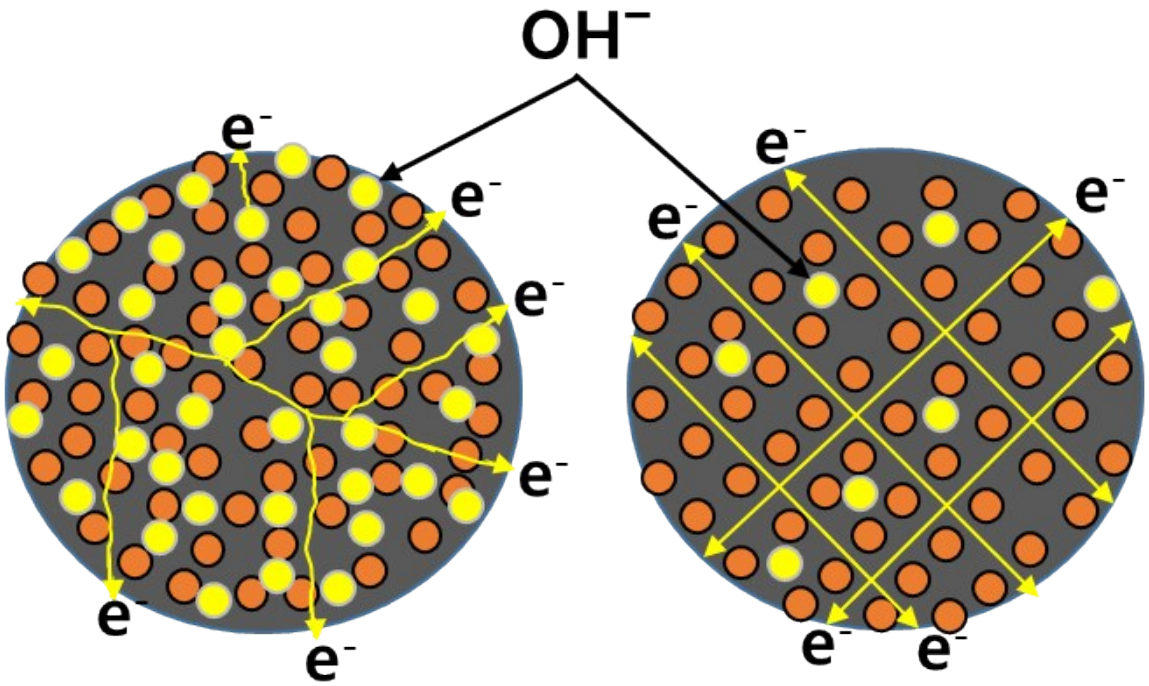

128

129 ***Figure S20****. The illustration shows the difference in the ion storage pattern and electron*

130 *transfer from the amorphous (left) and crystalline (right) CoPi/C composite.*

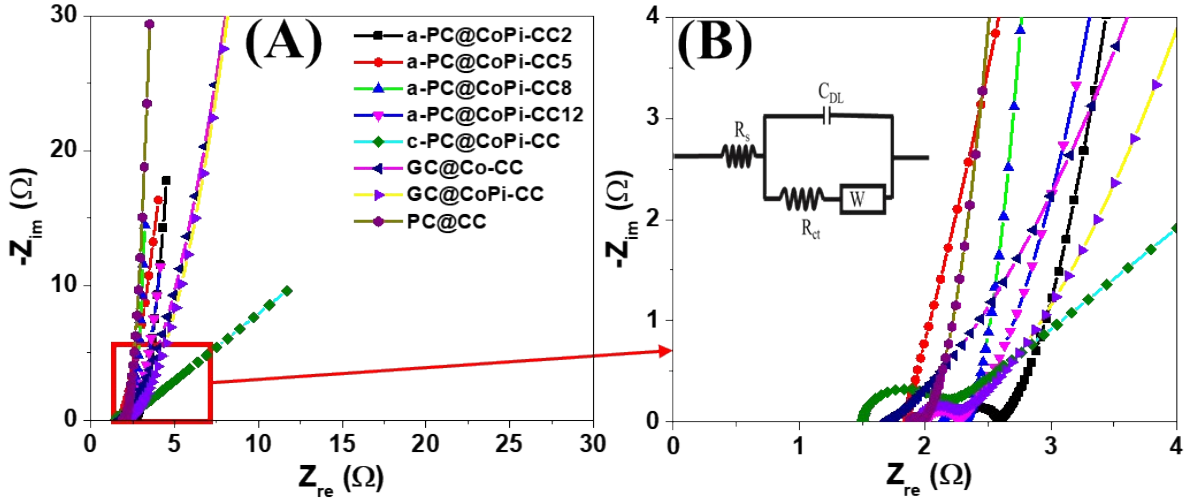

131

132 ***Figure S21.*** *Nyquist plots of different samples (A, B). In figure B, Nyquist plots of*

133 *Samples are magnified. Equivalent circuit model was used to fit the EIS spectra is shown in*

134 *the inset of B. ESR circuit is belongs to a-PC@CoPi-CC8.*

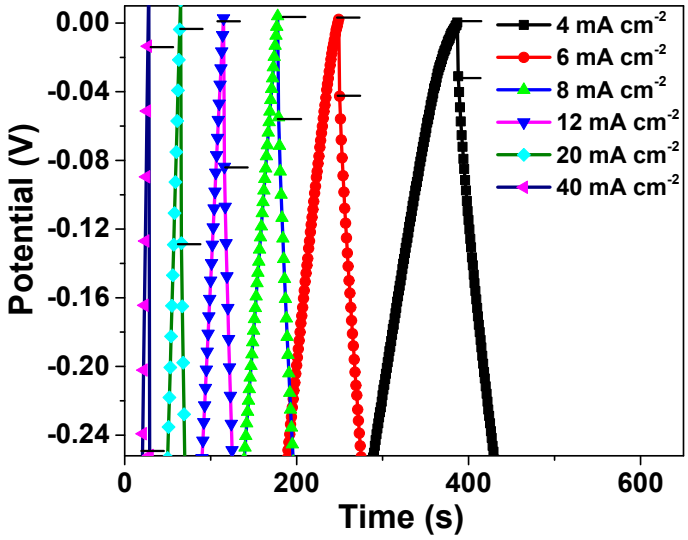

135

136 ***Figure S22.*** *iR drop evaluation of a-PC@CoPi-CC8.*

137

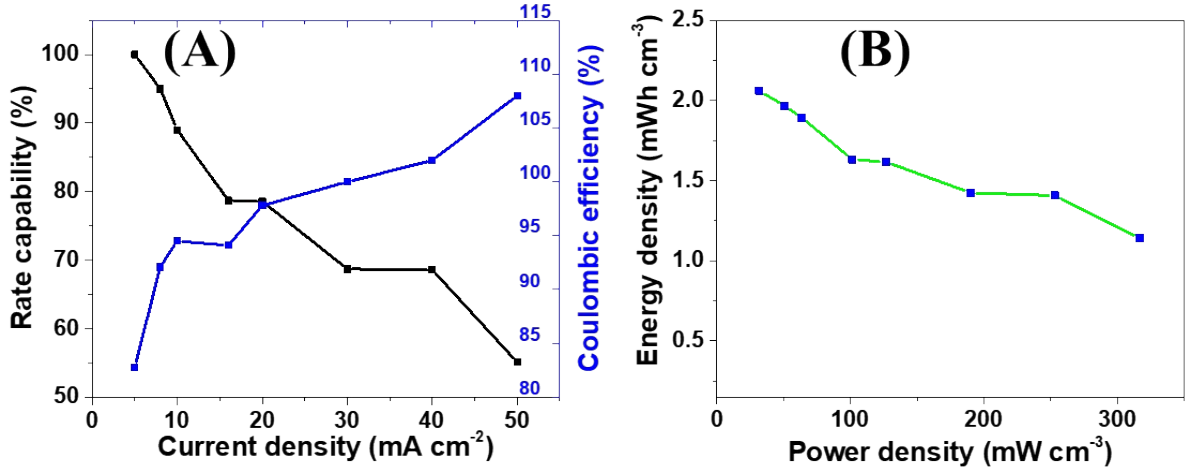

138

139 ***Figure S23.*** *Areal rate capability and coulombic efficiency of SSC device (A) and the graph*

140 *showing volumetric energy density vs power density of SSC device.*

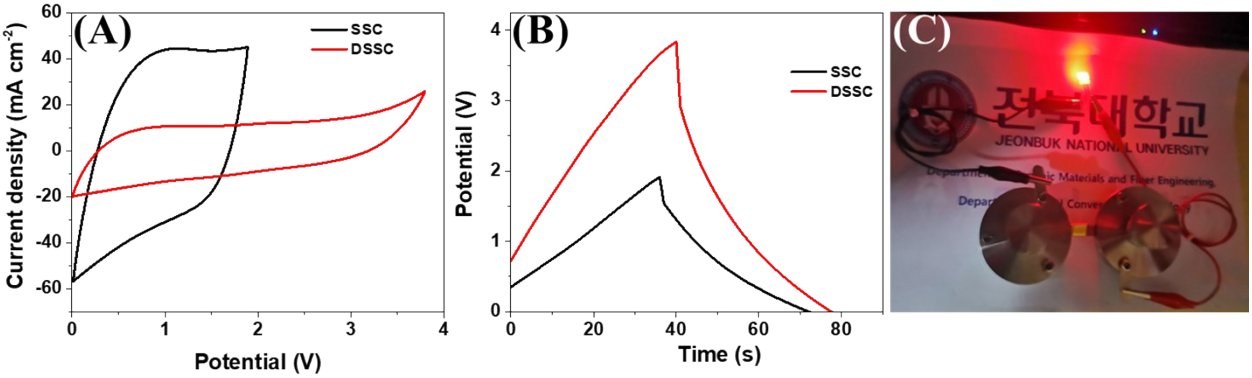

141

142 ***Figure S24.*** *CV profiles of SSC and DSSC collected at 50 mV s^{-1} (A), GCD curves of SSC and*

143 *DSSC device collected at 20 mA cm^{-2} (B) and image of a red LED powered by two SSC*

144 *supercapacitors in series. The supercapacitor devices were charged in around 40 s before LED*

145 *tests.*

146

147

148

149

150

Table S1. Comparison of areal capacitance, stability, and rate capability values of different electrode materials studied in this work.

Electrode materials	**Current density (mA cm^{-2})**	**Areal capacitance (F cm^{-2})**	**Capacity retention (%) at 10000 cycles**	**Rate capability (40 mA cm^{-2})**
a-PC@CoPi-CC-2	4	1.21 (606.1 F g^{-1} at 1 A g^{-1})		52.1%
	6	1.10		
	8	1.00		
	12	0.91		
	20	0.76		
	40	0.63		
a-PC@CoPi-CC-5	4	1.60 (322.0 F g^{-1} at 1 A g^{-1})		56.7%
	8	1.27		
	12	1.01		
	20	0.96		
	40	0.80		
a-PC@CoPi-	4	1.99 (248.7 F g^{-1} at		51.8%

CC-8		1 A g^{-1})		
	6	1.58		
	8	1.44		
	12	1.30		
	20	1.13	94.2%	
	40	1.05		
a-PC@CoPi-CC-12	4	2.15 (179.5 F g^{-1} at 1 A g^{-1})		50.8%
	6	1.87		
	8	1.71		
	10	1.62		
	12	1.54		
	20	1.33		
	40	1.08		
PC@CC	4	0.64 (128.6 F g^{-1} at 1.2 A g^{-1})		62.5%
	8	0.57		
	12	0.51		
	20	0.47		

	40	0.40		
c-PC@CoPi-CC	4	0.54		
	6	0.63		
	8	0.57	~76%	
	10	0.56		
	12	0.55		
	20	0.52		
	25	0.45		
GC@CoPi-CC (No PA)	1	0.25		64%
	2	0.25		
	3	0.24		
	4	0.23		
	6	0.21		
	8	0.20		
	10	0.20		
	20	0.16		
GC@Co-CC	4	0.10		33.3%
	6	0.08		

	8	0.07		
	10	0.06		

153

154 **Table S2.** Comparison with the capacitance reported in the literature.

S. N.	**Electrode materials**	**Specific capacity/capacitance**	**Electrolyte used**	**Use of binder**	**Stability (cycles)**	**Ref.**
1	PC@CoPi-CC2	1.21 F cm^{-2} at 4 mA cm^{-2} (606.1 F g^{-1} at 1 A g^{-1})	2 M KOH	Binder free		**This work**
2	PC@CoPi-CC5	1.60 F cm^{-2} at 4 mA cm^{-2} (322.0 F g^{-1} at 1 A g^{-1})	2 M KOH	Binder free		**This work**
3	PC@CoPi-CC8	1.99 F cm^{-2} at 4 mA cm^{-2} (248.7 F g^{-1} at 1 A g^{-1})	2 M KOH	Binder free	94.2% (10000)	**This work**
4	Porous carbon nanofibers (P-CNFs)	104 F g^{-1} (0.2 A g^{-1})	1 M (H_2SO_4)	Binder free	94% at 10 A g^{-1} (2000)	[4]
5	MnO_2/RGO/CF//GH	171 F cm^{-2} (0.5	1.0 M	Binde		[5]

	/CW	mA cm^{-2})	Na_2SO_4	r free		
6	PPy-Mxene composite	326.1 F g^{-1} at 0.1 A g^{-1} or 1.64 F cm^{-2} at 1 mA cm^{-2}	0.5 M H_2SO_4	Binder	>95% at 50 mV s^{-1} (30000)	[6]
7	PA assisted PANI gel	450 F g^{-1} at 0.5 A g^{-1}	1 M H_2SO_4	Binder free	83% (1000)	[7]
8	Fe_2O_3/PPy nanoarrays on CC	382.4 mF cm^{-2} (0.5 mA cm^{-2})	1 M Na_2SO_4	Binder free	97.2 % (5000)	[8]
9	Fe-P@CC	362 mF cm^{-2} at 1.2 mA cm^{-2}	3 M KOH	Binder	95% (10000)	[9]
10	P doped TiO_2	254 mF cm^{-2}	0.5 M Na_2SO_4	Binder free	63% (10000)	[10]
11	CoP/carbon	CoP@C (349.2 F g^{-1} at 1 A g^{-1})	3 M KOH	Binder	-	[11]
12	Fe/Fe_3O_4	20.8 mF cm^{-2} (10mV s^{-1})	3 M LiCl	Binder free	91.7% (2500)	[12]

13	Fe_2O_3@ACC electrode	2775 mF cm^{-2} in between −0.8 and 0 V at 1 mA cm^{-2}	3 M $LiNO_3$	Binder free	95% (4000)	[13]
13	Ni_2P@CF	1746 mF cm^{-2} at 5 mA cm^{-2}	1 M KOH	Binder free	-	[14]
14	(N, P-CQDs/rGO)	453.7 F g^{-1} at 1 A g^{-1}	6 M KOH	Binder	93.5% (10000)	[15]
15	$Fe_3P_2O_8$	200 F g^{-1} at 0.5 A g^{-1}	2 M KOH	Binder	35.0% (1000)	[16]

Table S3. Comparison with the R_s, R_{ct} and Z_w values of different samples including SSC.

Samples	R_s (ohm)	R_{ct} (ohm)	Z_W (ohm)
a-PC@CoPi-CC2	2.290	0.282	1.453
a-PC@CoPi-CC5	1.857	0.001	1.003
a-PC@CoPi-CC8	2.139	0.160	3.088
a-PC@CoPi-CC12	2.021	0.233	1.494
c-PC@CoPi-CC	1.507	0.592	0.294
GC@Co-CC	1.691	0.056	0.093
GC@CoPi-CC	1.962	0.288	0.354
PC@CC	1.878	0.092	1.843
SSC device-before stability	2.204	3.058	1.150
SSC device-after stability	2.065	3.475	0.078

References

1. A. P. Tiwari, S.-H. Chae, G. P. Ojha, B. Dahal, T. Mukhiya, M. Lee, K. Chhetri, T. Kim and H.-Y. Kim, *Journal of Colloid and Interface Science*, 2019, **553**, 622-630.
2. Y. Shu, B. Li, J. Chen, Q. Xu, H. Pang and X. Hu, *ACS Applied Materials & Interfaces*, 2018, **10**, 2360-2367.
3. C. Chen, N. Zhang, Y. He, B. Liang, R. Ma and X. Liu, *ACS Applied Materials & Interfaces*, 2016, **8**, 23114-23121.
4. Z. Dou, Z. Qin, Y. Shen, S. Hu, N. Liu and Y. Zhang, *Carbon*, 2019, **153**, 617-624.
5. Z. Zhang, F. Xiao and S. Wang, *Journal of Materials Chemistry A*, 2015, **3**, 11215-11223.
6. W. Zhao, J. Peng, W. Wang, B. Jin, T. Chen, S. Liu, Q. Zhao and W. Huang, *Small*, 2019, **15**, 1901351.
7. L. Pan, G. Yu, D. Zhai, H. R. Lee, W. Zhao, N. Liu, H. Wang, B. C. K. Tee, Y. Shi, Y. Cui and Z. Bao, *Proceedings of the National Academy of Sciences*, 2012, **109**, 9287.
8. L. Wang, H. Yang, X. Liu, R. Zeng, M. Li, Y. Huang and X. Hu, *Angewandte Chemie International Edition*, 2017, **56**, 1105-1110.
9. A. K. Yousef, Y. Kim, P. Bhanja, P. Mei, M. Pramanik, M. M. S. Sanad, M. M. Rashad, A. Y. El-

Sayed, A. A. Alshehri, Y. G. Alghamdi, K. A. Alzahrani, Y. Ide, J. Lin and Y. Yamauchi, *RSC Advances*, 2019, **9**, 25240-25247.

10. Y. Zhang, S. Duan, Y. Li, S. Zhang, Y. Wu, M. Ma, C. Tao, Z. Zhang, D. Qin and E. Xie, *Dalton Transactions*, 2020, DOI: 10.1039/C9DT04316K.

11. J. Gu, L. Sun, Y. Zhang, Q. Zhang, X. Li, H. Si, Y. Shi, C. Sun, Y. Gong and Y. Zhang, *Chemical Engineering Journal*, 2020, **385**, 123454.

12. L. Guohong, L. Ruchun and Z. Weijia, *Nano-Micro Letters*, 2017, **9**, 46.

13. J. Li, Y. Wang, W. Xu, Y. Wang, B. Zhang, S. Luo, X. Zhou, C. Zhang, X. Gu and C. Hu, *Nano Energy*, 2019, **57**, 379-387.

14. P. Sun, M. Qiu, J. Huang, J. Zhao, L. Chen, Y. Fu, G. Cui and Y. Tong, *Chemical Engineering Journal*, 2020, **380**, 122621.

15. J. Li, X. Yun, Z. Hu, L. Xi, N. Li, H. Tang, P. Lu and Y. Zhu, *Journal of Materials Chemistry A*, 2019, **7**, 26311-26325.

16. M. Liu, J. Li, W. Han and L. Kang, *Journal of Energy Chemistry*, 2016, **25**, 601-608.